Texas A&M University
Mechanical Engineering Department
Turbomachinery laboratory

A Novel FE Bulk-Flow Model Improving Predictions of Force Coefficients in Off-Centered Grooved Oil Seals

Research Progress Report to the Turbomachinery Research Consortium

TRC- SEAL-1-08

Adolfo Delgado
Research Assistant

Luis San Andrés
Mast-Childs Professor
Principal Investigator

June 2008

TEES project 32513/1519T7

Executive Summary

TRC-Seal-1-08

A Novel FE Bulk-Flow Model Improving Predictions of Force Coefficients in Off-Centered Grooved Oil Seals

Oil seals in centrifugal compressors reduce leakage of the process gas into the support bearings and ambient. Under certain operating conditions of speed and pressure, oil seals lock, becoming a source of hydrodynamic instability due to excessively large cross coupled stiffness coefficients. It is a common practice to machine circumferential grooves, breaking the seal land, to isolate shear flow induced film pressures in contiguous lands, and hence reducing the seal cross coupled stiffnesses. Exhaustive oil seal testing performed by Childs and students shows that an inner land groove, shallow or deep, does not actually reduce the cross-stiffnesses as much as conventional models predict. In addition, the tested grooved oil seals show overly large added mass coefficients; while predictive models, based on classical lubrication theory, miss entirely the fluid inertia effect.

A 2007 TRC report introduces a fluid inertia, bulk-flow model that properly accounts for the flow and moment transport at the groove-land interfaces. The novel model predicts with exactness the force coefficients of multiple-groove laminar flow oil seals at their centered condition. The analysis relies on an effective groove depth, different from the physical groove depth, which delimits the upper boundary for the flow induced by dynamic (fluid squeezing) motions in the grooved region of a seal.

The current report extends the bulk-flow analysis to predict the leakage, reaction forces and dynamic force coefficients of grooved oil seals operating at an off-centered (eccentric) locked condition. Predictions of rotordynamic force coefficients are compared to published test coefficients for a smooth land seal and a seal with a single groove seal with a depth of 15 times the land clearance (c=85.9 μm). The test data represents operation at 10 krpm and 70 bar oil feed pressure, and four journal eccentricity ratios (e/c= 0, 0.3, 0.5, 0.7). The enhanced model predicts accurately the smooth and grooved seals' leakage, reaction force, and rotordynamic force coefficients for the lowest eccentricities (e/c= 0, 0.3). The model yields moderate to good correlation with the test force coefficients for e/c=0.5. For the largest journal eccentricity, e/c=0.7, significant discrepancies between the predictions and experimental results arise. The test data

technical report does not offer details on operating conditions leading to large power dissipation that may have affected the lubricant properties and seal clearance.

The model completed is a significant improvement that predicts accurately the rotordynamic force coefficients of locked multiple-grooved oil seals. Prior to the current results, the cross-coupled stiffness coefficients of grooved oil seals were largely under predicted, and the direct added mass coefficients ignored or largely under predicted (up 10 times). The computational tool integrates a XLTRC^2 type GUI to the FEM solution of the flow equations.

Note: The P.I. edited this report five times, English and technical content, prior to its release to TRC members.

Table of Contents

List of Tables

List of Figures

Nomenclature

C_{ij}	Direct damping coefficients [N.s/m] $i,j=x,y$
c	Clearance [m]
c_η	Characteristic clearance [m]
d_η	Characteristic groove depth [m]
e_0	Journal eccentricity [m]
h	Film thickness [m]
L	Axial length [m]
K_{ij}	Direct stiffness coefficients [N/m] $i,j=x,y$
M_{ij}	Added mass coefficient [Kg] $i,j=x,y$
$\dot{m}_{x,z}$	Mass flow rates [kg/s]
N	Number of flow regions in flow domain
Nem	Number of elements (FEM mesh)
n_{pe}	Number of Nodes per element (FEM mesh)
P	Pressure [Pa]
P_X, P_Y	First-order pressure fields [Pa]
i	Imaginary number ($\sqrt{-1}$)
R	Journal radius [m]
Re_A	$V_A c\rho/\mu$. Axial flow Reynolds number
$\overline{\mathrm{Re}}_*$	$\rho\omega c_\eta^2/12\mu$. Modified squeeze film Reynolds number
s	Zeroth order pressure axial gradient [Pa/m]
t	Time [s]
V_x, V_z	Bulk flow velocities [m/s]
X,Y,Z	Inertial coordinate system [m]
x,z	Circumferential and axial coordinates [m]
Δe	Displacement amplitude [m]
ε	Eccentricity ratio (e/c)
μ	Absolute viscosity [Pa.s]
ν	Kinematic viscosity [m^2/s]
Ω	Rotor rotational speed [rad/s]
ω	Rotor whirling frequency [rad/s]
ρ	Oil density [kg/m^3]
θ	Angular coordinate [deg]
ψ	Interpolation functions (FEM)
Subscripts	
0	Zeroth order solution
exp.	Derived from experiments
g	groove
N	Last annular cavity section
model	Derived from predictions
α	α-th annular cavity section
σ	X,Y coordinates

I Introduction

Oil seals are used in centrifugal compressors to reduce leakage of the process gas into the support oil lubricated bearings as well as into ambient [1]. An oil seal, shown in Fig. 1, comprises of a floating ring and elastic support that, under certain operation conditions, may lock up and act as a hydrodynamic journal bearing [3]. These seals are known as potential sources of instability due to the generation of large cross-coupled stiffnesses [1, 4]. A common practice to minimize the destabilizing effect of oil seals is to machine circumferential grooves to isolate and divide the seal land into shorter length lands, thus reducing the hydrodynamic fluid film forces. To date, there are major discrepancies between predicted and experimental force coefficients obtained for grooved seals. Experimental results detailed in Refs. [1, 6, 7] show that incorporating circumferential grooves do reduce cross-coupled force coefficients but to a lesser extent than predictions otherwise indicate. Furthermore, experimental added mass coefficients are found to be very large and not modeled in common predictive tools.

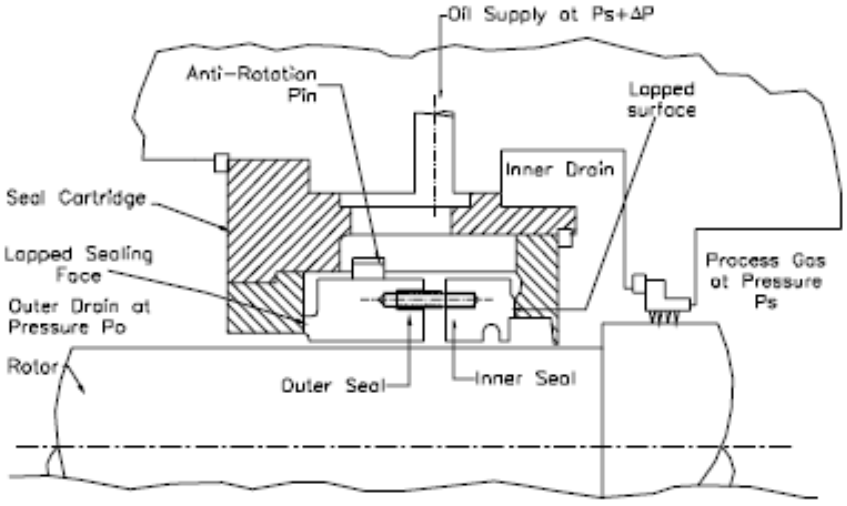

Figure 1 Oil seal ring assembly, Ref. [2]

A prior TRC report [8] introduces a novel analysis to obtain the force coefficients of centered grooved oil seals. The bulk-flow formulation determines seal force coefficients from an amplitude perturbation analysis about a centered position. Extending the original bulk flow analysis, this report details the implementation of a finite element method to obtain the oil seal force coefficient for journal (rotor) off-centered conditions.

The following review presents the analytical and experimental work on laminar-flow grooved oil seals.

II Literature Review

The archival literature for laminar flow oil grooved seals is rather scant [1,9]. Most of the work has been conducted to analyze turbulent flow annular pressure seals typical in high pressure compressors and pumps [9]. This literature review includes the current available computational tools and experimental results valid for laminar-flow grooved oil seals, i.e. axial flow Reynolds number ($Re_A = V_a * c/\nu$) $\leq$ 2000, with V_a as the axial mean flow velocity, c as the film clearance, and ν is the kinematic viscosity.

Analytical work

Semanate and San Andrés [3] present an isoviscous bulk flow analysis to predict force coefficients of a grooved oil seal operating under either laminar or turbulent flow regimes and not accounting for fluid inertia terms. The analysis includes surface roughness, fluid inertia and viscous effects at the seal inlet plane, and variable clearance (i.e. tapered seal). The bulk flow equations are solved for small amplitude motions using a perturbation analysis and an iterative finite difference scheme. The force coefficients are presented in terms of the ring eccentricity ratio for three cases: single land, two lands and three lands. The numerical results indicate that both the cross-coupled stiffnesses and direct damping coefficients are substantially reduced. These findings imply that the grooves effectively separate the seal lands, thus reducing the seal force coefficients. However, the whirl frequency ratio (WFR), a stability indicator, remains relatively constant, and thus there is not significant improvement of the seal rotordynamic stability characteristics. Regarding the entrance effects due to viscous and inertia effects, the predictions indicate that such effects are of importance only for high pressure applications.

Baheti and Kirk [4] analyze the dynamic forced response of grooved oil seals including thermal effects but still neglecting fluid inertia. The coupled pressure and temperature transport equations, developed in terms of a perturbation analysis for small amplitude journal motions, are modeled with a finite element scheme. The study includes arc and square groove geometries located at the seal mid-land length. The numerical

results show a reduction of 40% in the direct damping and cross-coupled stiffness coefficients of an oil seal when including a square groove with a groove depth to clearance ratio (d_g/c) equal to 6. On the other hand, when using a deeper groove (d_g/c = 15) the force coefficients are reduced by a factor of 4 by adding a single groove, and by 10 when adding two grooves. Thus, for the latter case, the results indicate that an inner groove effectively isolates the pressure distribution of contiguous film lands.

San Andrés and Delgado [8] present a bulk-flow fluid inertia analysis to predict the force coefficients of grooved oils seals and squeeze film dampers operating at their centered position. A perturbation analysis yields zeroth and first order flow equations at each individual flow region (land and grooves) of constant clearance (c). The authors present an analytical solution for circular centered journal orbits of small amplitude. The model relies on defining an effective groove depth that represents the actual upper boundary of the dynamic (squeeze) flow. A parametric study using multiple effective groove depths (d_η) show that there is an excellent correlation between the predicted and experimental force coefficients of a grooved oil seal [6] for a narrow range of effective groove depths. Specifically, for a short length and shallow groove at the mid-land of the seal, predictions of added mass, cross-coupled stiffness, and damping coefficients correlate best with experimental data [6] when using a fraction (50% or less) of the actual groove depth. Most importantly, the predictions demonstrate that the inner groove in the oil seal does not isolate the adjacent film lands.

Experimental work

Childs *et al.* [1] identify experimentally the rotordynamic force coefficients and measure the leakage of smooth land and grooved oil seals operating under laminar flow conditions. The authors aim to quantify the influence of inner-land grooves on the rotordynamic coefficients of oil seals and to evaluate the accuracy of existing predictive models. Ref. [1] includes a detailed description of smooth and grooved oil seals and their operating features, and a comprehensive literature review of prior work conducted on oil seals operating in the laminar flow regime. Particularly, the authors indicate that, prior to their publication, the only published experimental work on laminar-flow oil seals was conducted by Kaneko [10] on smooth land seals. In Ref. [1], static and dynamic force coefficients are identified for a smooth seal, a 1-groove seal, and a 3-groove seal (with d_g/c = 6). The experimental force coefficients for the smooth seal correlate well with

predictions from an annular seal model given in Ref. [11], except for the added mass coefficient that the analysis underestimates by a factor of about 10. The authors note that the large volume of the oil supply central groove may explain the large discrepancy. However, pressure measurements at both the feed groove and exit cavity show no dynamic pressure oscillations. The experimental force coefficients for the grooved oil seals are largely underestimated by the model of Semanate and San Andrés [3]. The test results suggest that, contrary to the accepted assumptions, inner-land grooves are not deep enough to isolate the hydrodynamic pressures from contiguous seal film lands.

Childs *et al.* [6] present experimental results evidencing the effect of groove depth on the dynamic force response and leakage of a test oil seal. Rotordynamic force coefficients are identified for four seals, including a smooth land seal and three seals with a single groove at the middle of the land. The three grooved seals present different groove depth to clearance ratios; d_g/c = 5, 10, and 15. The identified seal force coefficients and leakage are presented as a function of the seal journal eccentricity for three speeds and three oil supply pressures. The test results indicate that the seal force coefficients decrease as the groove depth increases, except for the added mass coefficients. However, predictions based on Ref. [3] largely underestimate the grooved seal oil cross-coupled stiffnesses and direct damping coefficients even for the test seal with the deepest groove. Thus, the experiments reveal that, even for a groove depth to clearance ratio as large as 15, a groove does not completely isolate the hydrodynamic pressures of the two adjacent seal lands (i.e. for the cross-coupled stiffness coefficients: K_{xy} (2 lands) ≠ ¼ K_{xy} (1 land), and the direct damping coefficients: C_{xx}(2 lands) ≠ ¼ C_{xx}(1 land) as predictions reported in [3]. In addition, the experimental results also show relatively large added mass coefficients that increase as the groove depth increases. However, a prediction of added mass coefficient, based on a classical lubrication model [12], yields only 2.8 kg (i.e. 10 times smaller than the experimental value). On the other hand, the predicted added mass coefficients obtained with the novel model in Ref.[8] show a remarkable correlation with the test data.

III Analysis

The literature review reveals the need for an improved model that properly predicts the force coefficients of a (laminar flow) grooved ring seal for eccentric journal operation.

This deficiency is addressed by updating the bulk flow model advanced in Ref. [8] for off-centered journal operation using a finite element analysis. The derivation of the bulk flow equation for the oil seal follows.

Bulk flow formulation

The following bulk flow model is an extension of the original analysis in Ref. [8] to determine the fluid forces developed in multi-groove annular seal cavities. The model sets a rotating journal whirling with small amplitude motions about an off-centered (eccentric) position. As in Ref. [8], the model applies to both smooth land and grooved oil seals operating in the laminar flow regime. Specifically, the formulation is detailed for the case of annular cavities with axially symmetric groove configurations, including a central feeding groove, as shown in Fig. 2. This geometry is selected to allow direct comparisons with the experimental data in Ref. [7].

The multiple groove seal is divided into separate flow regions of uniform clearance. In case of a groove, the depth is an effective groove depth (d_η), which differs from the actual physical groove depth. This concept is explained later while describing the boundary conditions for the FE model solution.

The following derivation applies to each individual flow region with constant clearance, and with a local coordinate system whose origin is at the entrance of the corresponding grooved or ungrooved flow region. Figure 3 depicts the journal and the coordinate system used in the analysis for small journal motions about an off-centered position.

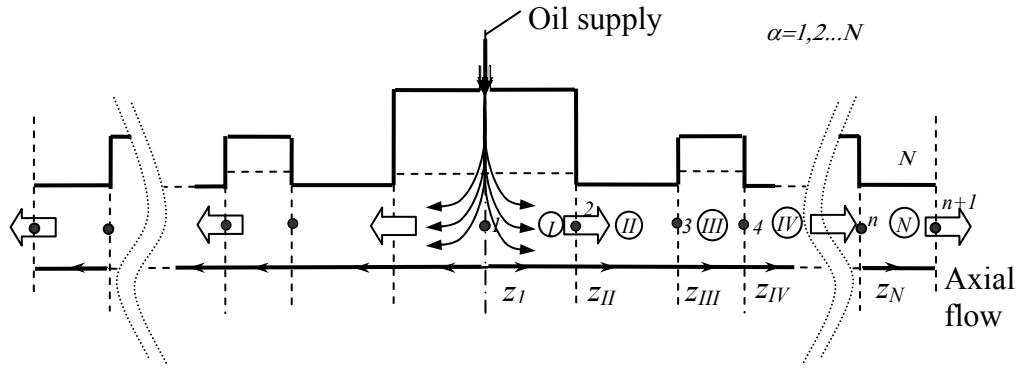

Figure 2 Schematic view of grooved annular cavity divided into flow regions

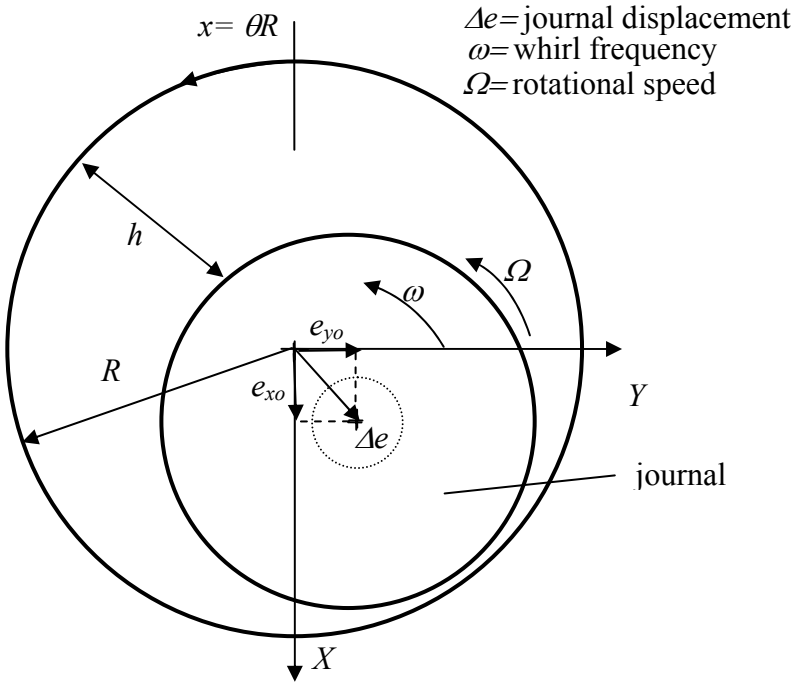

Figure 3 View of rotating and whirling journal and coordinate system for bulk-flow analysis

Within each individual flow region the mass flow rates in the circumferential (x) and axial (z) directions are:

$$\dot{m}_{x_\alpha} = \rho h_\alpha V_{x_\alpha} \; ; \; \dot{m}_{z_\alpha} = \rho h_\alpha V_{z_\alpha} \qquad \alpha = I, II, ...N \tag{1}$$

where h_α is the film thickness, ($V_{x_\alpha}, V_{z_\alpha}$) are bulk-flow velocities in each flow region α, and ρ is the lubricant density.

The bulk-flow continuity and moment transport equations without fluid advection terms are [13]:

$$\frac{\partial}{\partial x}\left(\dot{m}_{x_\alpha}\right) + \frac{\partial}{\partial z_\alpha}\left(\dot{m}_{z_\alpha}\right) + \frac{\partial}{\partial t}\left(\rho h_\alpha\right) = 0 \tag{2}$$

$$-h_\alpha \frac{\partial P_\alpha}{\partial x} = k_x \frac{\mu}{h_\alpha}\left(V_{x_\alpha} - \frac{\Omega R}{2}\right) + \frac{\partial\left(\dot{m}_{x_\alpha}\right)}{\partial t} \tag{3}$$

$$-h_\alpha \frac{\partial P_\alpha}{\partial z_\alpha} = k_z \, \mu \frac{V_{z_\alpha}}{h_\alpha} + \frac{\partial\left(\dot{m}_{z_\alpha}\right)}{\partial t} \; ; \quad \alpha = I, II, ...N \tag{4}$$

with k_x=k_z=12 for laminar flow. Above, μ is the lubricant viscosity and P_α is the pressure at each flow region. Equations (3) and (4) are rewritten as:

$$\begin{aligned} \dot{m}_{x_\alpha} &= -\frac{\rho h_\alpha^{\,3}}{k_x \mu}\frac{\partial P_\alpha}{\partial x} - \frac{\rho h_\alpha^{\,2}}{k_x \mu}\frac{\partial\left(\dot{m}_{x_\alpha}\right)}{\partial t} + \frac{\rho h_\alpha \Omega R}{2}; \\ \dot{m}_{z_\alpha} &= -\frac{\rho h_\alpha^{\,3}}{k_z \mu}\frac{\partial P_\alpha}{\partial z_\alpha} - \frac{\rho h_\alpha^{\,2}}{k_z \mu}\frac{\partial\left(\dot{m}_{z_\alpha}\right)}{\partial t} \quad ; \quad \alpha = I, II, \ldots N \end{aligned} \tag{5}$$

Differentiating $\dot{m}_{x_\alpha}$ with respect to x, and $\dot{m}_{z_\alpha}$ with respect to z_α, adding both equations, and disregarding second order terms yields a Reynolds-like equation for the film pressure of an incompressible fluid [11]

$$\frac{\partial}{\partial x}\left(h_\alpha^{\,3}\frac{\partial P_\alpha}{\partial x}\right) + \frac{\partial}{\partial z_\alpha}\left(h_\alpha^{\,3}\frac{\partial P_\alpha}{\partial z_\alpha}\right) = 12\mu\frac{\partial}{\partial t}\left(h_\alpha\right) + 6\mu R\Omega\frac{\partial}{\partial x}\left(h_\alpha\right) + \left(\rho h_\alpha^{\,2}\right)\frac{\partial^2}{\partial t^2}\left(h_\alpha\right) \qquad \alpha = I, II, \ldots N \tag{6}$$

The journal describes motions of small amplitude $(\Delta e_X\,,\ \Delta e_Y) << c_{\eta_\alpha}$ and frequency ω about an static position (e_{Xo}, e_{Yo}). The film thickness (h_α) equals [13]

$$h_\alpha = h_{0_\alpha} + e^{i\omega t}\left\{\Delta e_X\ \cos(\theta) + \Delta e_Y \sin(\theta)\right\} = h_{0_\alpha} + e^{i\omega t}\ \Delta e_\sigma h_\sigma;\ \ i = \sqrt{-1};\ \sigma = X, Y \qquad \alpha = I, II, \ldots N \tag{7}$$

with

$$h_{0_\alpha} = c_{\eta_\alpha} + e_X\cos(\theta) + e_Y\sin(\theta) = c_{\eta_\alpha} + e_{\sigma_0}h_\sigma;\ \ h_X = \cos(\theta), h_Y = \sin(\theta) \tag{8}$$

and $c_{\eta_\alpha} = \left(c + d_{\eta_\alpha}\right)$ is the effective clearance over the grooved flow regions. Note that d_{η_α} is the effective groove depth, and $c_{\eta_\alpha} = c$ in an ungrooved (seal land) flow region. The pressure is expressed as a superposition of a zeroth order field (P_o) and first order (dynamic) fields ($P_{X_\alpha}, P_{Y_\alpha}$)

$$P_\alpha = P_{0_\alpha} + \Delta e_\sigma\ P_{\sigma_\alpha}\ e^{i\omega t} \quad ; \quad \alpha = I, II, \ldots N \tag{9}$$

Substitution of Eqs. (7) and (9), into Eq. (6) gives the zero$_{th}$ order equations for the equilibrium pressure

$$\frac{\partial}{\partial x}\left(h_{0_\alpha}^{\,3}\frac{\partial P_{0_\alpha}}{\partial x}\right)+\frac{\partial}{\partial z_\alpha}\left(h_{0_\alpha}^{\,3}\frac{\partial P_{0_\alpha}}{\partial z_\alpha}\right) = 6\mu R\Omega\frac{\partial}{\partial x}\left(h_{0_\alpha}\right) \qquad \alpha = I, II, \ldots N \tag{10}$$

and the first order equations for journal dynamic displacements along the X and Y directions

$$\frac{\partial}{\partial x}\left(h_\alpha^{\,3}\frac{\partial P_{\sigma_\alpha}}{\partial x}\right)+\frac{\partial}{\partial z_\alpha}\left(h_\alpha^{\,3}\frac{\partial P_{\sigma_\alpha}}{\partial z_\alpha}\right)= 12\,i\,\mu\,\omega\left\{1+i\,\overline{\mathrm{Re}}_{*_\alpha}\right\} h_\sigma + 6\mu\Omega R\frac{dh_\sigma}{dx}$$
$$-\frac{\partial}{\partial x}\left(3h_{0_\alpha}{}^2 h_\sigma\frac{\partial P_{0_\alpha}}{\partial x}\right)-\frac{\partial}{\partial z}\left(3h_{0_\alpha}{}^2 h_\sigma\frac{\partial P_{0_\alpha}}{\partial z}\right); \tag{11}$$
$$\sigma = X, Y;\ \alpha = I, II, \ldots N$$

where $\overline{\mathrm{Re}}_{*_\alpha} = \dfrac{\rho\omega c_{\eta_\alpha}^2}{12\,\mu}$ is a local squeeze film Reynolds number. Once Eq. (10) and Eq. (11) are solved, the fluid film reaction forces at a static journal position (e_{Xo}, e_{Yo}) are

$$F_{\sigma 0} = \sum_{\alpha=1}^{N}\int_0^{L_\alpha}\int_\theta h_\sigma P_{0_\alpha} R\,d\theta dz_\alpha; \quad {}_{\sigma=X,Y;} \tag{12}$$

The seal force coefficients are also obtained by integrating the dynamic pressure fields over the flow domain [13],

$$K_{\sigma\beta_\alpha} - \omega^2 M_{\sigma\beta_\alpha} + \mathrm{i}\omega C_{\sigma\beta_\alpha} = -\sum_{\alpha=1}^{N}\int_0^{L_\alpha}\int_\theta h_\sigma P_{\beta_\alpha} R\,d\theta dz_\alpha; {}_{\sigma,\beta=X,Y}\ ; h_X = \cos(\theta), h_Y = \sin(\theta)$$
$$\alpha = I, II, \ldots N \tag{13}$$

Finite element solution

The procedure implemented for solving the Reynolds-like Eq. (11) with the finite element method (FEM) is similar to that in Refs. [13,14]. The implementation of the current development into a FORTRAN® code follows from modifying an existing code that predicts force coefficient for smooth seals without including inertia effects [3]. Without loss of generality, the solution is presented for a symmetric oil seal with an inlet groove and a single mid-land groove similar to the seal tested in Ref. [7]. A similar solution can be applied to multi-groove seals.

Following the discretization of the domain into elements (Ω^e), as shown in Fig. 4, the static and dynamic pressure fields are represented as the linear combination of nodal values $\overline{P}_i^e$ within each element as

$$P_0^e = \sum_{i=1}^{n_{pe}} \Psi_i \overline{P}_{0_i}^e \ , \ P_\sigma^e = \sum_{i=1}^{n_{pe}} \Psi_i \overline{P}_{\sigma_i}^e \ ; \ _{\sigma=X,Y} \tag{11}$$

where ψ^e are bilinear interpolation functions. The equation to be solved for each element follows from the representation of the fluid differential equations (10, 11) in its variational or weak form [13] using the interpolation functions as weight functions.

`

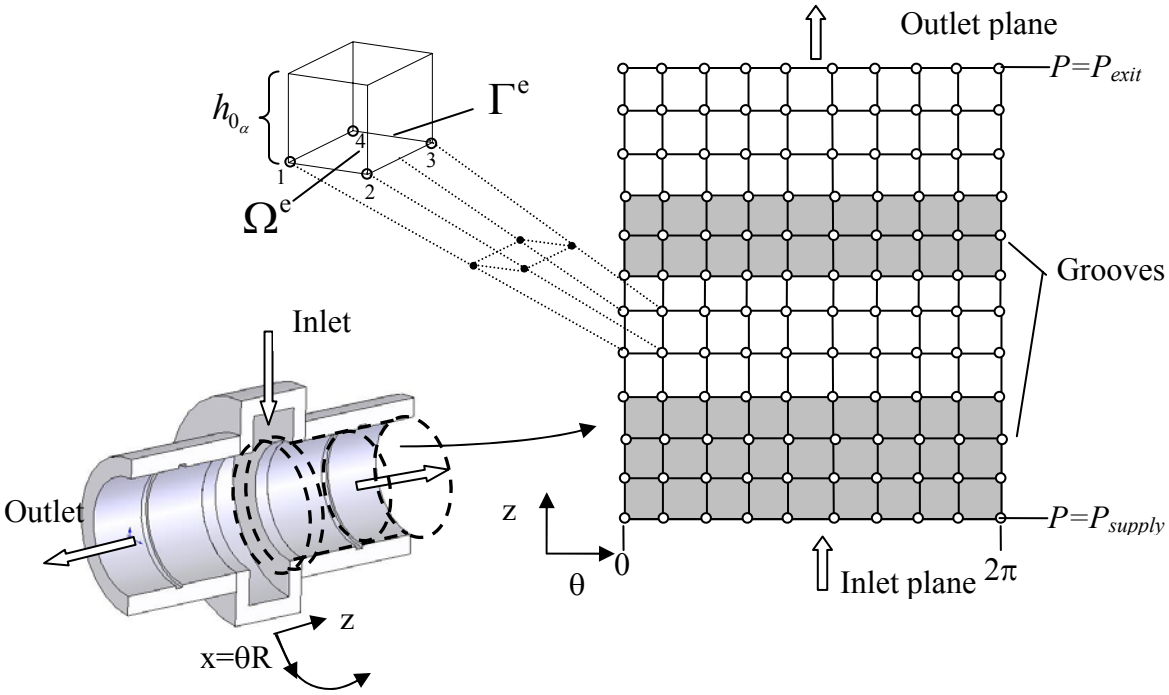

Figure 4 Coordinate system and sample mesh for oil seal FEM computational code

The weak variational form of Eq. (10) for the zeroth order pressure yields

$$\sum_{j=1}^{n_{pe}} k_{ij}^e \overline{P}_{0_j}^e = -q_i^e + f_i^e \tag{12}$$

with

$$k_{ij}^{e} = \iint_{\Omega^e} \left(\frac{h_{0_\alpha}^3}{12\mu} \right)^e \left\{ \frac{\partial \Psi_i}{\partial x} \frac{\partial \Psi_j}{\partial x} + \frac{\partial \Psi_i}{\partial z} \frac{\partial \Psi_j}{\partial z} \right\}^e dx\, dz \tag{13}$$

$$f_{0_i}^{e} = \frac{\Omega R}{2} \iint_{\Omega^e} h_{0_\alpha} \frac{\partial \Psi_i^e}{\partial x}\, dx\, dz \tag{14}$$

$$q_{0_i}^{e} = \oint_{\Gamma^e} \Psi_i^e q_{n_0} d\Gamma^e \;\; ; \;\; \text{with} \;\; q_{n_0} = -\frac{h_{0_\alpha}^3}{12\mu} \frac{\partial P_0}{\partial n} + \frac{h_{0_\alpha} \Omega R}{2} n_x \tag{15}$$

Similarly for the first order perturbed pressure fields, P_X and P_Y, the set of equations for the nodal pressures in a finite element are

$$\sum_{j=1}^{n_{pe}} k_{ij}^{e} \overline{P}_{\sigma_j}^{e} = f_{\sigma_i}^{e} - \sum_{j=1}^{n_{pe}} S_{\sigma_{ij}}^{e} \overline{P}_{0_j}^{e} - q_{\sigma_i}^{e} \;\; ; \;\; {}_{\sigma = X,\, Y} \tag{16}$$

where

$$f_{\sigma_i}^{e} = \iint_{\Omega^e} h_\sigma \left[\frac{\Omega R}{2} \frac{\partial \Psi_i^e}{\partial x} + \frac{\rho \omega^2}{12\mu} \Psi_i^e \; h_{0_\alpha}^2 \right] dx\, dz \; - \mathbf{i}\, \omega \iint_{\Omega^e} h_\sigma \left[\Psi_i^e \right] dx\, dz \tag{17}$$

$$S_{\sigma_{ij}}^{e} = \iint_{\Omega^e} \left(\frac{3 h_{0_\alpha}^2}{12\mu} \right)^e \left\{ \frac{\partial \Psi_i}{\partial x} \frac{\partial \Psi_j}{\partial x} + \frac{\partial \Psi_i}{\partial z} \frac{\partial \Psi_j}{\partial z} \right\}^e h_\sigma \; dx\, dz \tag{18}$$

$$q_{\sigma_i}^{e} = \oint_{\Gamma^e} \Psi_i^e q_{n_\sigma} d\Gamma^e ; \;\; q_{n_\sigma} = \left(-\frac{h_{0_\alpha}^3}{12\mu} \frac{\partial P_\sigma}{\partial n} - \frac{3 h_{0_\alpha}^2}{12\mu} h_\sigma \frac{\partial P_0}{\partial n} \right) + \frac{\Omega R}{2} h_\sigma n_x \tag{19}$$

with n as the normal vector to the boundary Γ^e of an element. Note that Eq. (17) includes the temporal fluid inertia term (second term in first integral). The integrals in Eq. (13) through Eq. (19) are evaluated numerically over a master element ($\hat{\Omega}$) with normalized coordinates (isoparametric element). Reddy and Gartling [15] detail the coordinate transformation and numerical integration procedure using Gauss-Legendre quadrature formulas.

Equations (12) and (16), for each element of the flow domain, are assembled to form a linear system of equations represented as

$$\left[k\right]_{Global}\left\{\bar{P}_0\right\}_{Global}=\left\{Q_\gamma\right\}_{Global}+\left\{F_\gamma\right\}_{Global}\quad;\quad\gamma:0$$

$$\left[k\right]_{Global}\left\{\bar{P}_\gamma\right\}_{Global}=\left\{Q_\gamma\right\}_{Global}+\left\{F_\gamma\right\}_{Global}+\left[S\right]_{Global}\left\{\bar{P}_0\right\}_{Global}\;;\;\gamma:X,Y \tag{20}$$

where

$$\left[k\right]_{Global}=\bigcup_{e=1}^{Nem}\left[k\right]^e,\ \left\{Q_\gamma\right\}_{Global}=\bigcup_{e=1}^{Nem}\left\{q_\gamma\right\}^e,\ \left\{F_\gamma\right\}_{Global}=\bigcup_{e=1}^{Nem}\left\{f_\gamma\right\}^e,\ \gamma{:}0,X,Y. \tag{21}$$

The resulting global fluidity matrix $\left[k\right]_{Global}$ is symmetric and can be easily decomposed into its upper and lower triangular form, i.e.

$$\left[k\right]_G=\left[L\right]_G\left[U\right]_G=\left[L\right]_G\left[L\right]_G^T \tag{22}$$

Thus, once the **L, L**^{T} and **F** matrices are obtained, and stating the pressure at the inlet and exit planes of the flow domain, a process of back- and forward-substitutions renders the discrete zeroth order pressure field $\left\{\bar{P}_0\right\}_G$. Using the results from the fluidity matrix and the zeroth order pressure field, the first order pressure field, $\left\{\bar{P}_\gamma\right\}_G$, are obtained. The selection of the appropriate boundary conditions, based on the physics of the problem, is essential for obtaining the force coefficients in the grooved seal geometry.

Boundary Conditions

Figure 5 shows the mesh for ½ a flow domain on an oil seal with an inlet (supply) groove and an inner groove, and the nodes of interest to enforce boundary conditions.

Both the zeroth and first order fields are periodic in the circumferential direction,

$$\bar{P}_\gamma\left(\theta,z\right)=\bar{P}_\gamma\left(\theta+2\pi,z\right)\;;\;_{\gamma=0,\,X,\,Y} \tag{23}$$

The fluid pressure must be greater than the lubricant cavitation pressure (P_{cav}). In the current analysis, the Gumbel condition of oil cavitation is enforced for the zeroth and first order pressure fields.

Note that Eqs. (15) and (19) automatically satisfy the flow continuity at the boundary between a smooth land and groove, for example. Hence, no special considerations in regard to flow matching are required. Other boundary conditions are:

Zeroth Order Pressure Field

A) Constant static pressure at inlet plane ($z= 0$). This condition is set to the lower nodes of elements along the inlet plane.

$$\bar{P}_0^e\Big|_{z=L} = P_{\text{supply}} \tag{24}$$

B) Constant static pressure at exit plane ($z= L$). This condition is set to the upper nodes of elements along the exit plane.

$$\bar{P}_0^e\Big|_{z=0} = P_{\text{exit}} \tag{25}$$

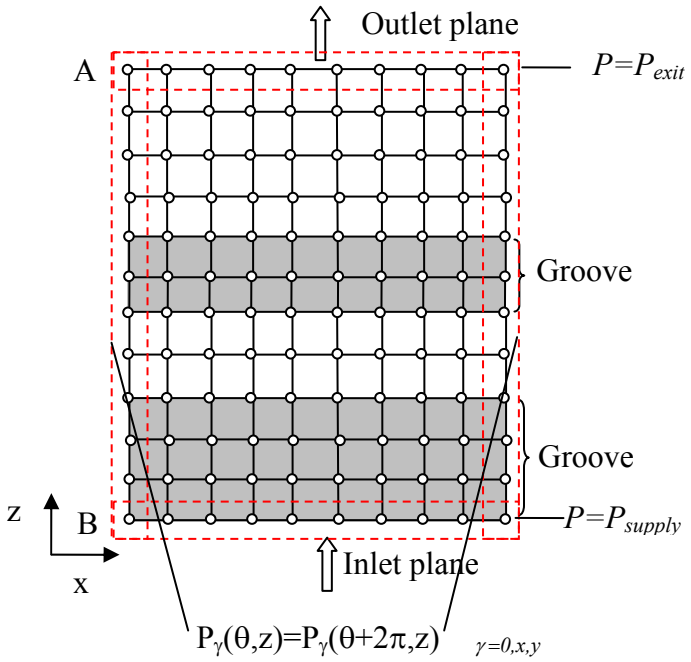

Figure 5 FEM mesh depicting nodes of interest for implementation of boundary conditions

First Order Pressure Fields

A) Null dynamic pressure at exit plane ($z= L$). While the static pressure is constant, it is assumed that there is not generation of dynamic pressure at the exit (discharge) plane. This condition is set to the upper nodes of elements along the exit plane.

$$\bar{P}_\gamma^e\Big|_{z=L} = 0 \tag{26}$$

B) At the inlet plane (feed or supply central groove) the axial flow induced by the dynamic (fluid squeezing) motions is set to zero due to axial symmetry.

$$q_z\Big|_{z=0} = 0 \tag{27}$$

This boundary condition implies that the "perturbed" axial flow does not cross the middle plane and that there is a non-zero dynamic pressure field at this plane. This is a Neumann type B.C. implemented by treating the nodes at inlet plane as internal nodes.

Effective groove depth

As advanced in Ref. [8], the laminar flow pattern at the groove is characterized by a recirculation region and a thru flow region. These regions are divided by a stream line that is considered to act as a physical boundary. Figure 5 shows a representation of the streamlines pattern for a pressure driven flow through a (symmetric) annular cavity with a supply groove and two mid-land grooves. The figure also depicts a close-up of CFD simulations of the pressure driven flow at the mid-land groove for two groove depths (10*c* and 15*c*). In this configuration the flow pattern at the supply and mid-land grooves is characterized by two regions, a recirculation region and a thru flow region. Furthermore, the dividing streamlines for the 10c and 15c groove depths present a similar penetration depth. In the proposed analysis, the streamlines dividing the two flow regions are assumed to act as physical boundaries delimiting the domain for the flow induced due to dynamic (fluid squeezing) journal motions. Thus, the fluid film clearance at the groove is represented in terms of an effective clearance $c_\eta = (d_\eta + c)$, with d_η as an effective groove depth and c as the clearance of the ungrooved portion or land.

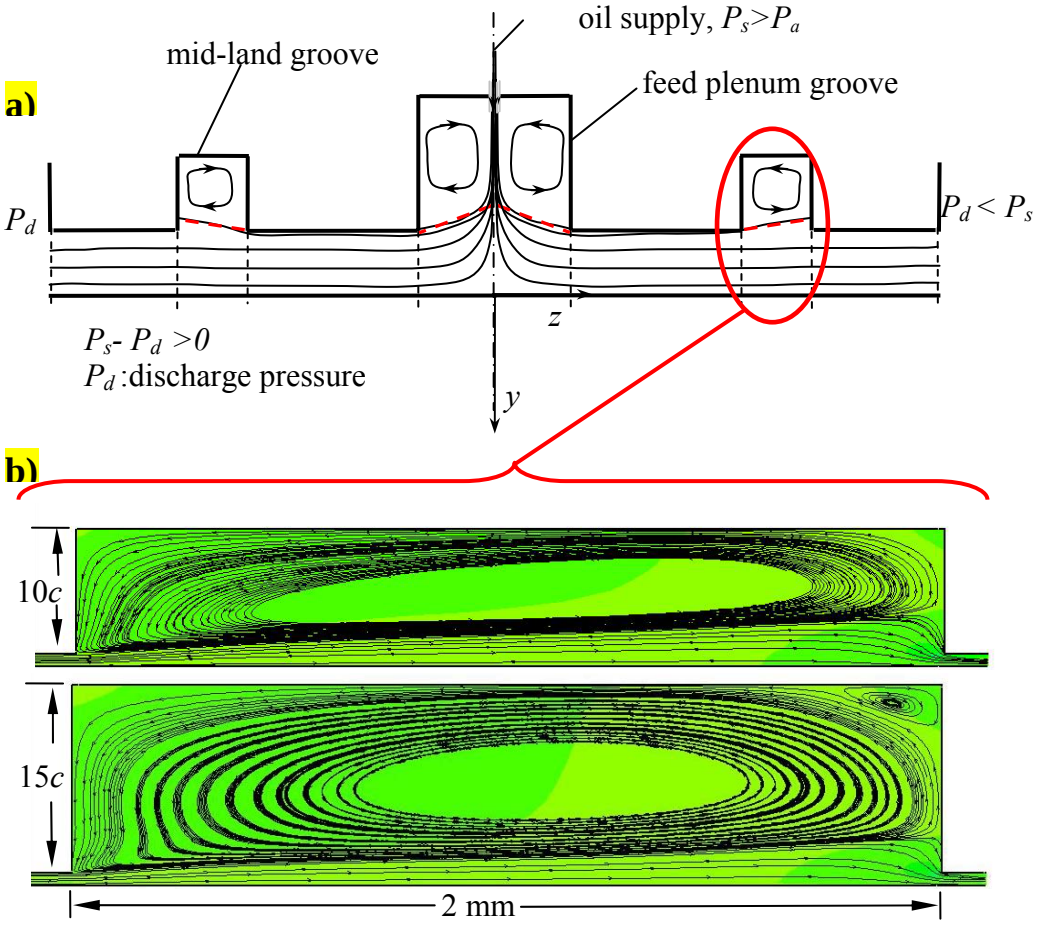

Figure 6 a) Schematic view of streamlines in axially symmetric grooved annular cavity ($\Delta P = P_s - P_d$). b) CFD simulation of pressure driven streamlines across a 10c and 15c circumferential mid-land groove in an oil seal tested in Ref. [7]. (c= 86 mm, ω=10000 RPM, D= 117 mm)

Excel program interface

The MS Excel® user interface is named XLFEGLOSeal® (Excel Finite element grooved laminar oil seal), as depicted in Fig. 7. The user inputs include:

-Fluid properties: Density and viscosity

-Operating conditions: Inlet and outlet pressures, static journal eccentricity.

-Geometry: Rotor diameter, clearance, groove depth, number of grooves, inlet and outlet land length, inter-groove length, groove length. The mid-land groove depth is set to the actual physical value for groove depths less than (6c), considering that the effective groove depth and actual groove depth are relatively similar. For deeper short mid-land grooves, as those found in oil seals, the pressure driven flow streamlines remain

relatively constant regardless of the actual depth, as shown in Fig. 6. For this case, a constant effective groove depth of d_η=6c is used.

The code outputs direct and cross-coupled force coefficients, seal reactions forces and leakage as a function of shaft speed journal eccentricity. The program can handle multiple groove configurations.

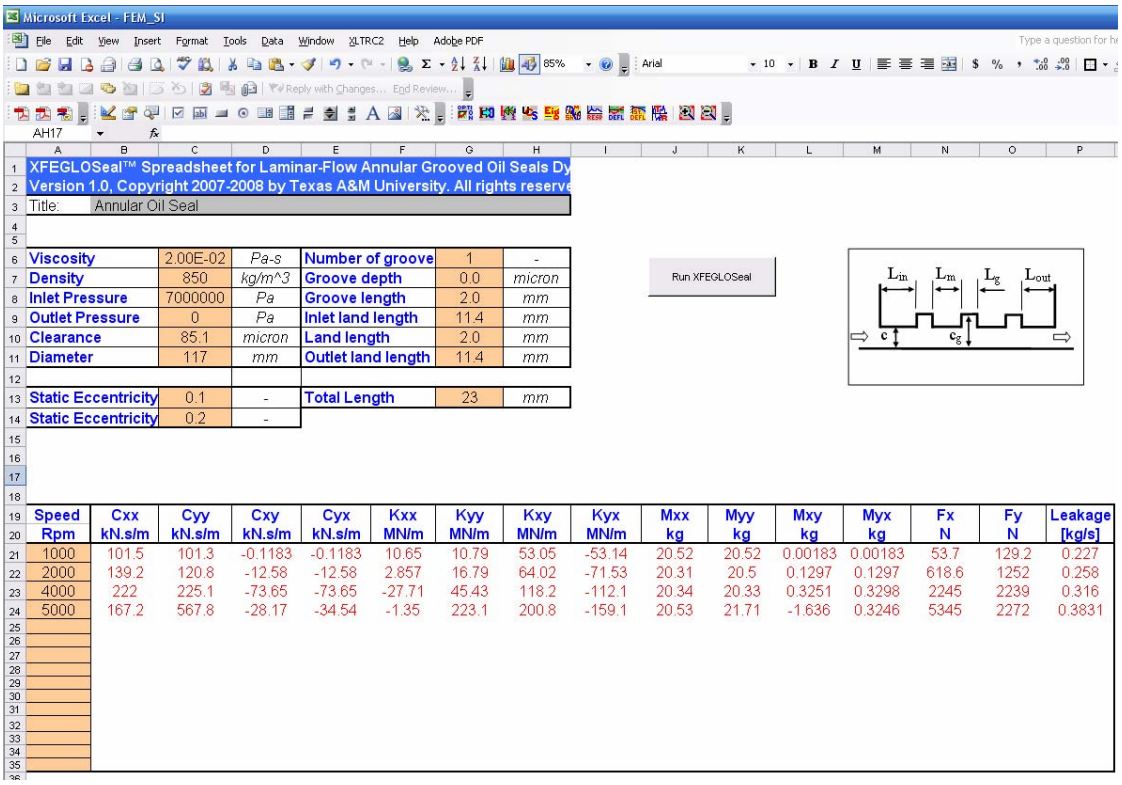

Figure 7 Graphical user interface for XLFEGLOSeal® code (SI units)

IV Model Predictions and Validation to Test Data

This section presents comparisons of experimental and predicted damping, stiffness and mass coefficients for the oil ring seal tested by Graviss [7]. Figure 8 depicts the actual dimensions of the test seal, and Table 1 lists the seal physical dimensions, fluid properties, operating conditions, and number of elements of the FE mesh. Figure 9 shows the actual journal locus obtained from four measured journal eccentricities. Considering that the external load is along the Y direction, the closeness of the journal center to the Y axis (i.e. small journal attitude angle) clearly indicates the presence of oil cavitation, in particular for the largest eccentricity ratios.

As in the tests, the analysis reports results for half of the axially symmetric grooved seal configuration. Published test data and predictions follow for a smooth land oil seal

and for the same seal land with an inner groove of 15*c* depth. Following the results of the parametric study in Ref. [8], the effective clearance for the inlet oil supply (central) groove is set to 10*c*. This effective clearance presents the best correlation with all the force coefficients obtained for the smooth seal (i.e. no mid-land groove). For the oil seal with a mid-land groove, the inlet oil supply groove effective groove depth remains constant and the inner land groove effective clearance is set to 7*c*.

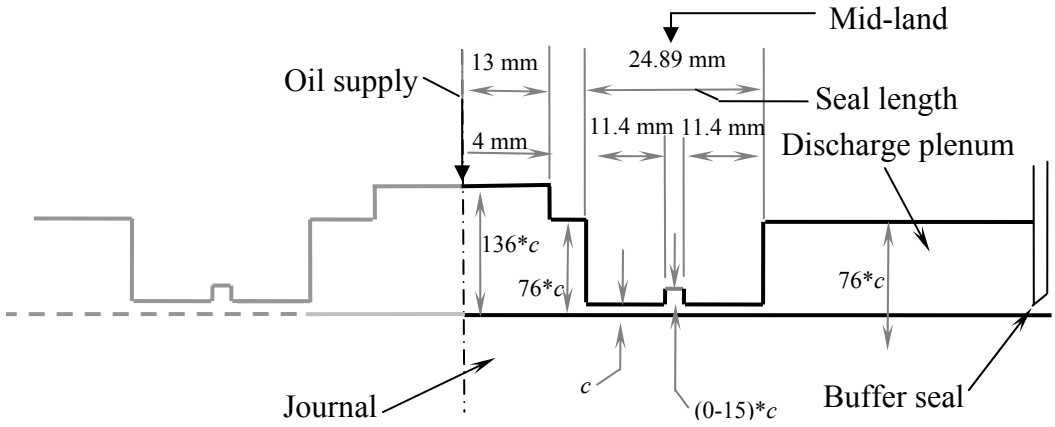

Figure 8 Configuration of parallel oil seals tested in Ref. [6]

Table 1 Oil seal configuration, operating conditions fluid properties and number of elements for FE mesh

Dimensions	
Journal Diameter	117 mm
Seal length	24.89 mm
Clearance	85.9 μm
Inlet groove length	17 mm
Inlet groove depth	136*c*
Inner land groove length	2 mm
Inner land groove depth	0-15*c*
Parameters	
Shaft speed	4000-10000 rpm
Oil density	850 kg/m^3
Static eccentricity	0-0.7
Oil viscosity (smooth seal)	0.016 Pa.s (54 ^{0}C)
Oil viscosity (grooved seal)	0.019 Pa.s (49 ^{0}C)
Supply pressure	70 bar
FEM mesh (elements)	
Circumference	60
Seal land	12
Inlet groove	12
Inner land groove	6

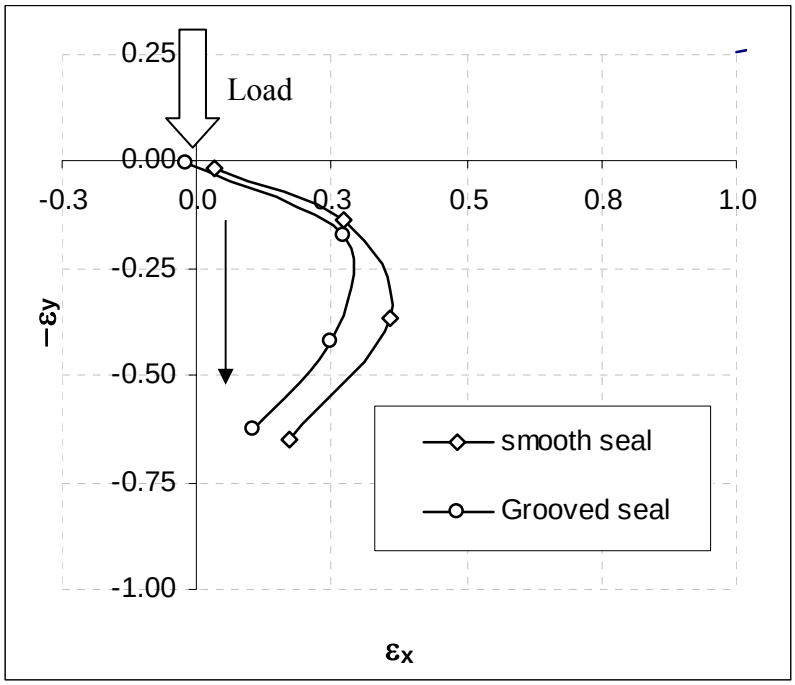

Figure 9 Measured journal centerline locus for smooth and grooved seal (c_g =15c). (70 bar, 10000 rpm) [7]

Figure 10 shows the seal reaction forces versus the static journal eccentricity. Predictions and experimental results present good correlation for journal eccentricities up to e/c = 0.5 for the grooved and smooth seals. For the largest journal eccentricity (e/c=0.7), predictions are within 20 % of the experimental results for the smooth seal. On the other hand, the reaction force of the grooved seal is underpredicted by a factor of 2 for the largest journal eccentricity. For the largest journal eccentricities the oil temperature is expected to significantly increase due to the small film thickness (i.e. large shear forces and power loss). Thus, the actual seal clearance and oil properties for the largest eccentricity may differ significantly from the nominal values and have a large uncertainty. However, Ref. [7] does not detail information on the exit temperature or measurements of *hot* clearances (immediately after testing). Presently, predictions are compared with test data for the low to mid-range journal eccentricities (i.e. ε= 0, 0.3, 0.5) only.

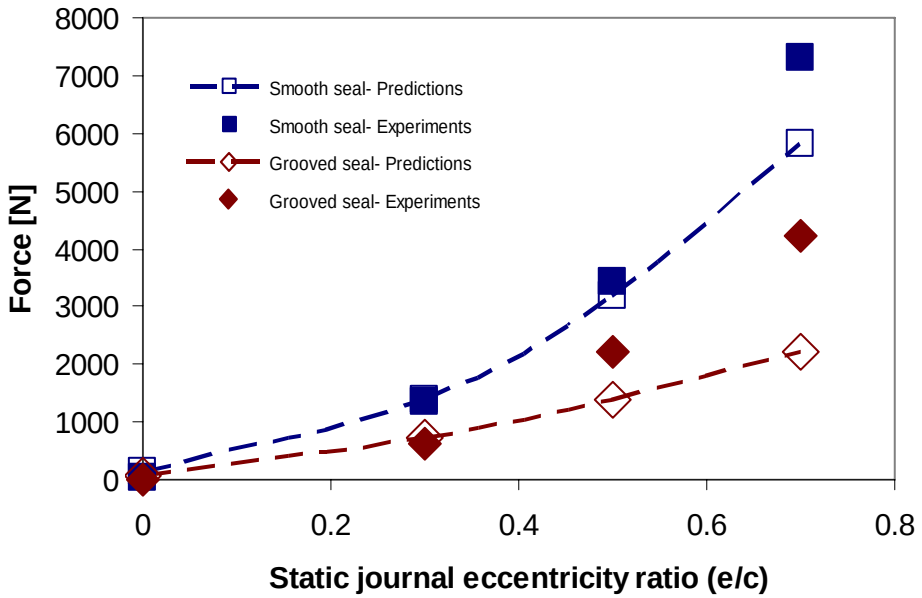

Figure 10 Seal reaction forces. Experiments for smooth seal and seal with inner land groove (c_g= 15c), 10000 rpm, 70 bar [7]. Predictions for smooth seal and seal with inner land groove (c_η = 7c)

Figures 11 and 12 depict the direct and crossed-coupled stiffness coefficients ($K_{ij\ ;\ i,j=x,y}$) versus the operating journal eccentricity, respectively. The predictions correlate well with the test data for the lower journal eccentricity ratios (ε= 0, 0.3). For the 50 % eccentricity ratio there are discrepancies. The differences can be attributed in part to the lack of knowledge in actual clearance and oil exit temperature, not reported in Ref. [7].

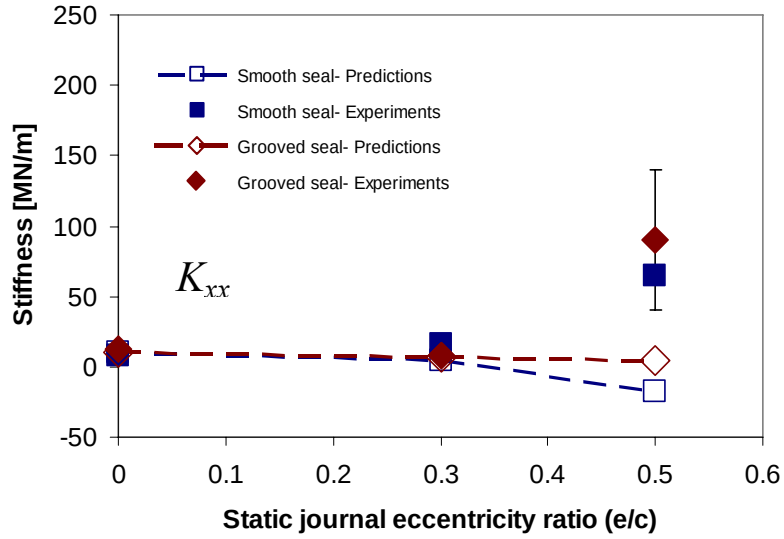

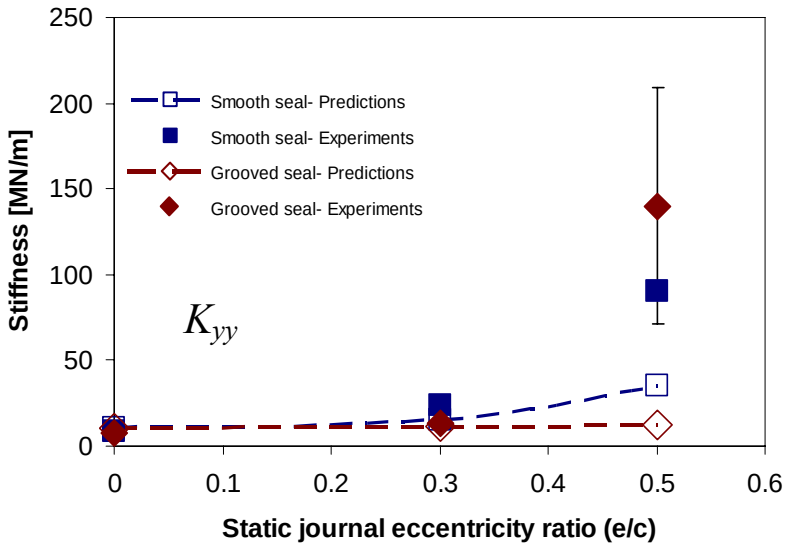

Figure 11 Direct stiffness coefficient (K_{ii}) versus eccentricity. Experiments for smooth seal and seal with inner land groove (c_g= 15c), 10000 rpm, 70 bar [7]. Predictions for smooth seal and seal with inner land groove (c_η = 7c)

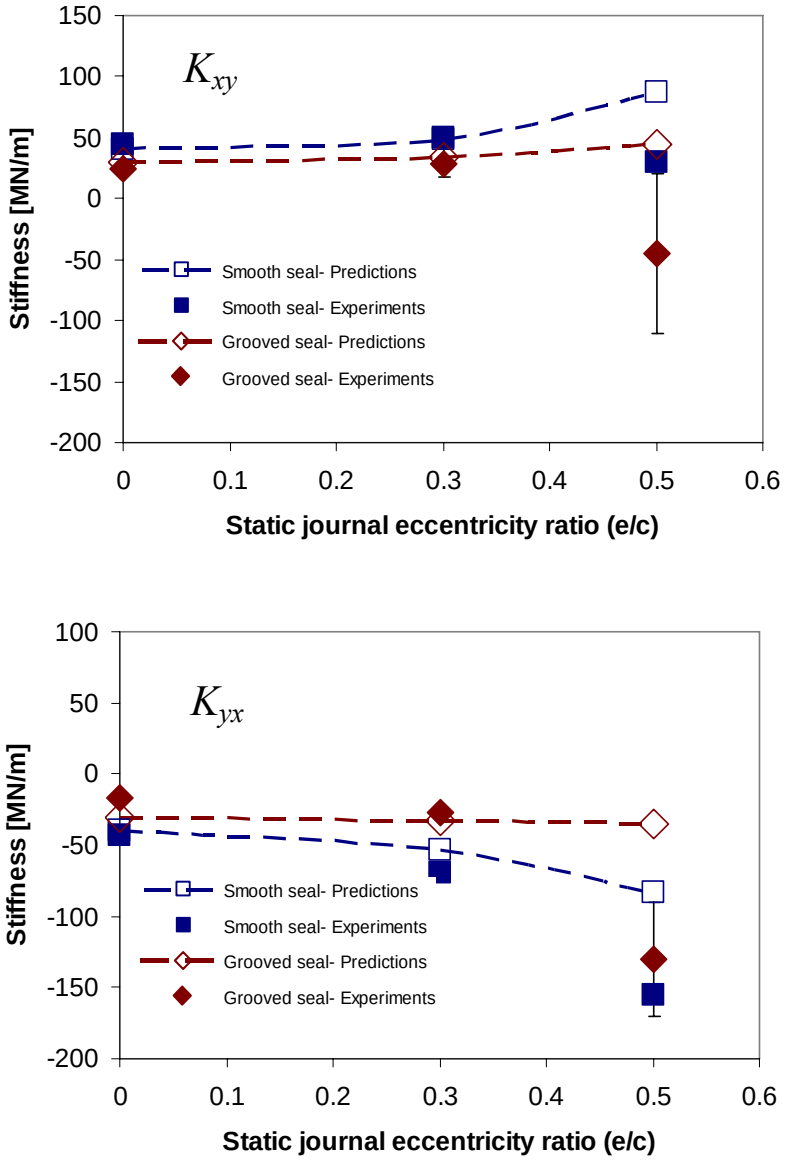

Figure 12 Cross-coupled stiffness coefficients (K_{ij}) versus eccentricity. Experiments for smooth seal and seal with inner land groove (c_g= 15c), 10000 rpm, 70 bar [7]. Predictions for smooth seal and seal with inner land groove (c_η = 7c)

Figure 13 show the cross-coupled stiffness coefficients versus rotor speed for two journal eccentricities (e/c=0, 0.3). The predictions are in good correlation with the experimental results. In particular, the model adequately predicts the reduction of the cross-coupled coefficients after adding the inner groove to the smooth land seal.

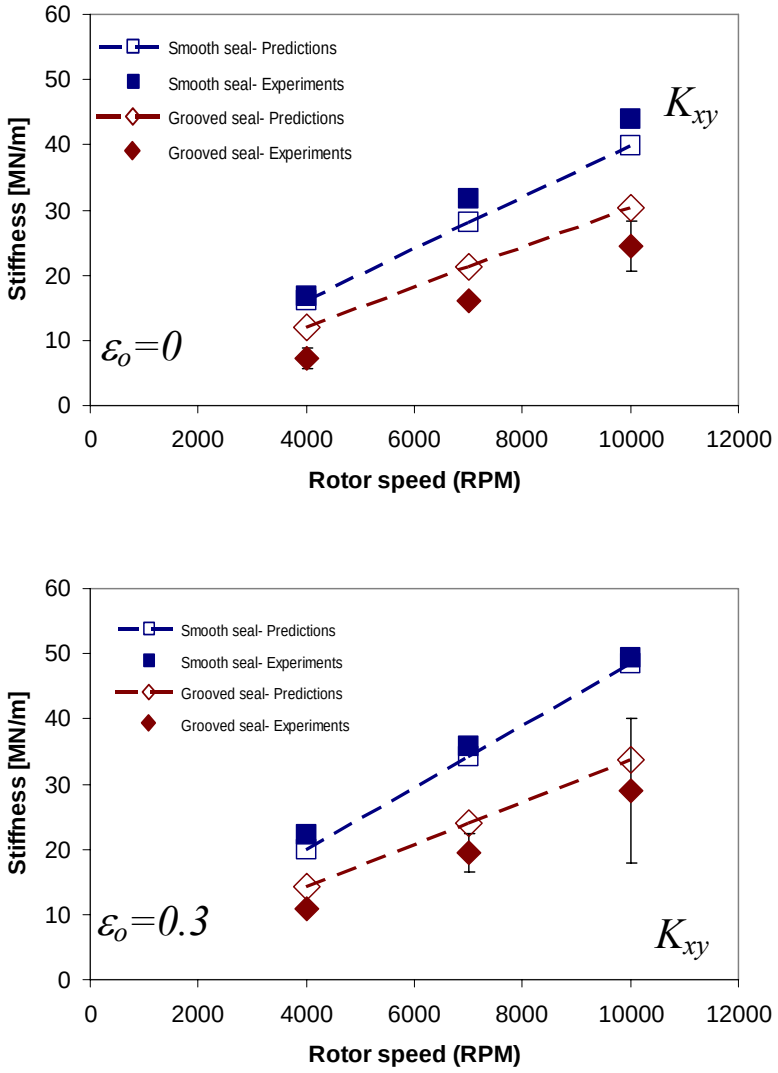

Figure 13 Cross-coupled stiffness coefficients (K_{xy}) versus shaft speed at two journal eccentricities (0, 0.3). Experiments for smooth seal and seal with inner land groove (c_g= 15c), 10000 rpm, 70 bar [7]. Predictions for smooth seal and seal with inner land groove (c_η = 7c)

Figures 14 and 15 present the direct and cross-coupled damping coefficients (C_{ij} ; $_{i,j=x,y}$) versus static journal eccentricity ratio, respectively. The direct damping coefficients (C_{xx}, C_{yy}) show excellent correlation for the all the eccentricity ratios, except for the C_{xx} coefficient of the smooth seal that is 20% underpredicted for e/c=0.5. The cross-coupled coefficients are much smaller than the direct damping coefficients and present moderate to good correlation for the different test journal eccentricities.

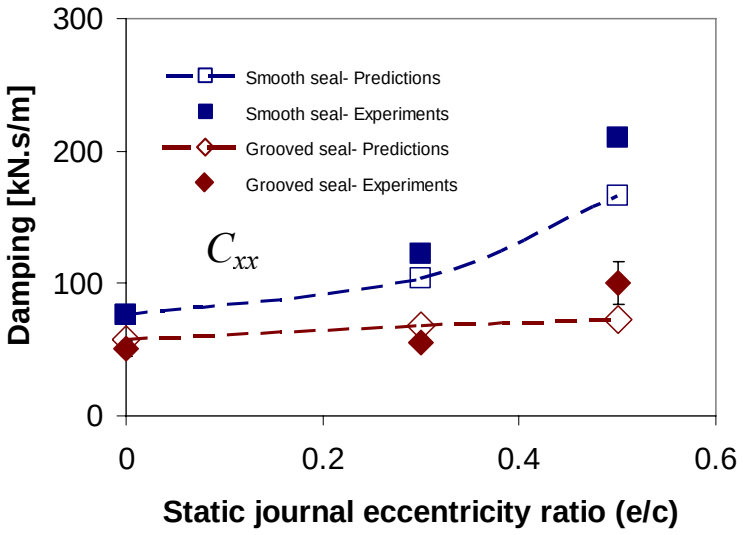

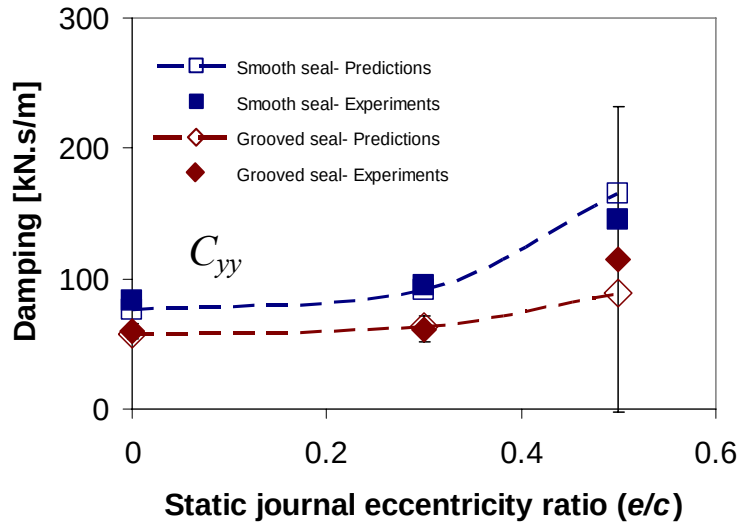

Figure 14 Direct damping coefficients (C_{ii}) versus eccentricity. Experiments for smooth seal and seal with inner land groove (c_g= 15c), 10000 rpm, 70 bar [7]. Predictions for smooth seal and seal with inner land groove (c_η = 7c)

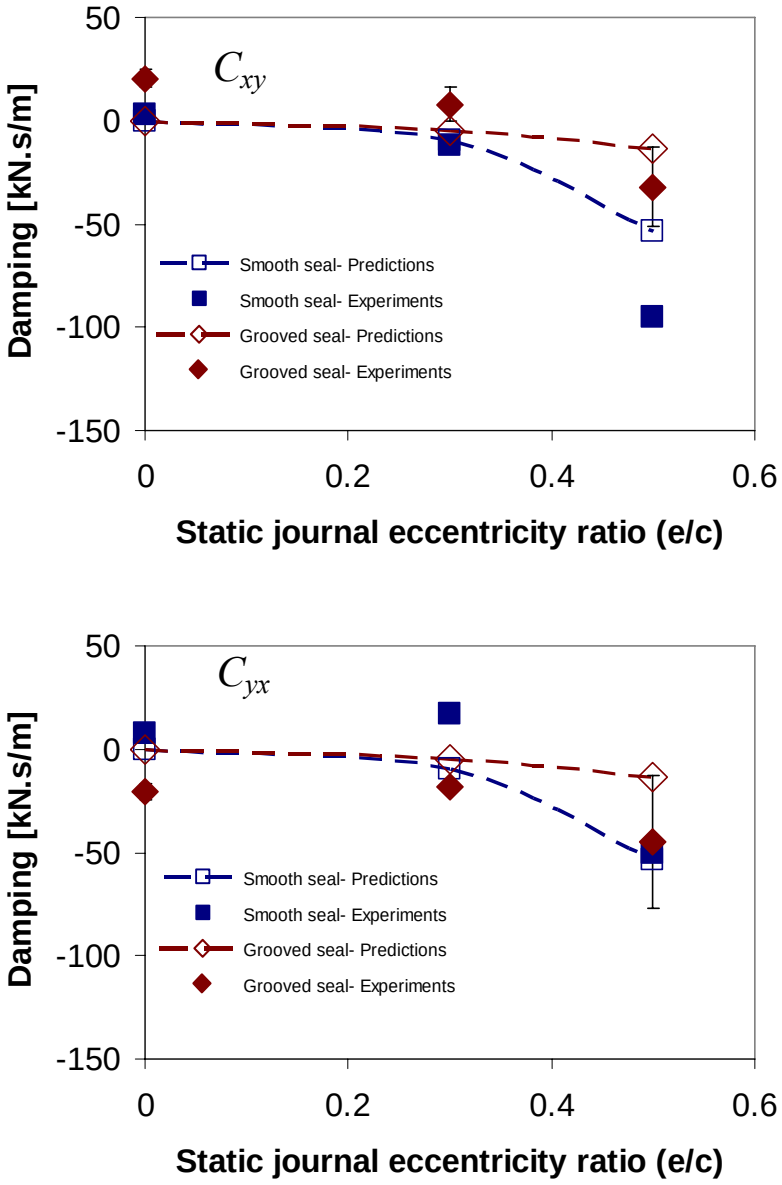

Figure 15 Cross-coupled damping coefficients (C_{ij}) versus eccentricity. Experiments for smooth seal and seal with inner land groove (c_g= 15c), 10000 rpm, 70 bar [7]. Predictions for smooth seal and seal with inner land groove (c_η = 7c)

Figure 16 depicts the direct added mass coefficients versus the static journal eccentricity ratio. Predicted and experimental cross-coupled added mass coefficients (M_{xy}, M_{yx}) are nearly null and not presented. The direct added mass coefficients (M_{xx}, M_{yy}) present good correlation with the experimental data. In particular, the analysis predicts a larger added mass coefficient for the grooved oil seal as the experiments also reveal. Note

that the predicted added mass coefficient is nearly constant for all the test journal eccentricities.

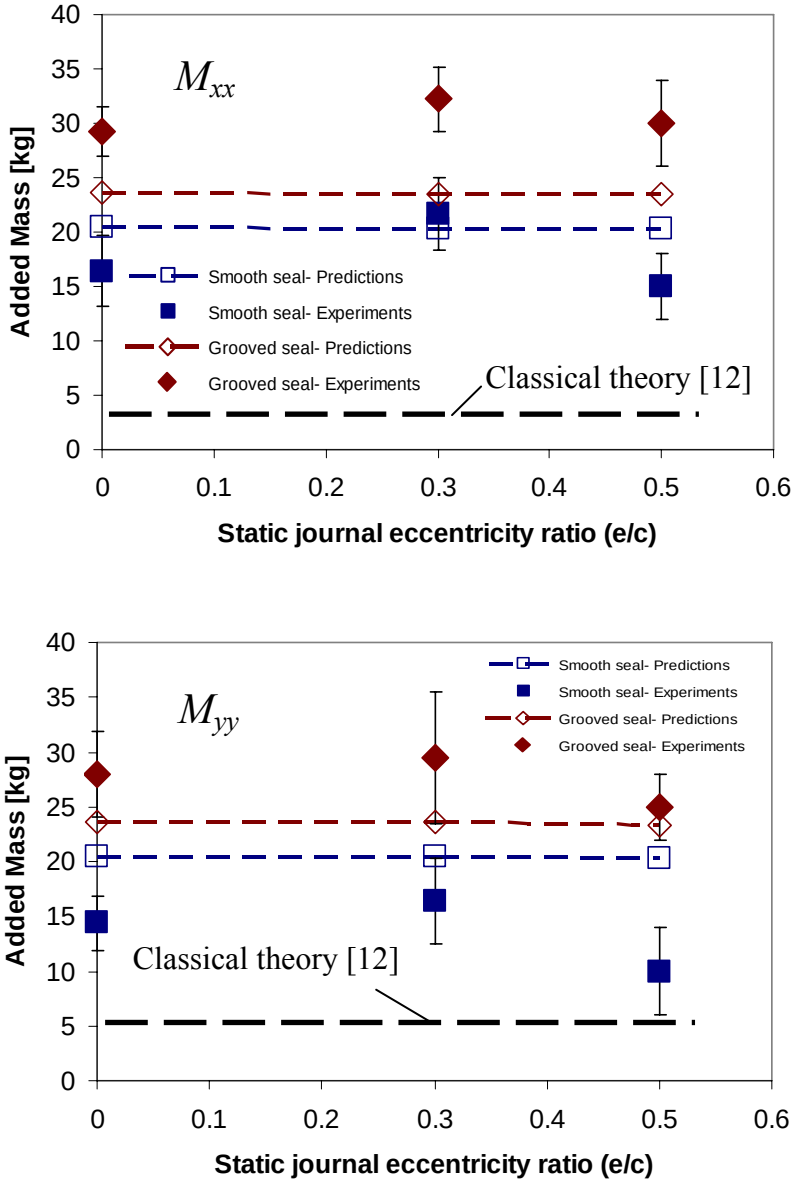

Figure 16 Added Mass coefficient (M_{xx}, M_{yy}) versus eccentricity. Experiments for smooth seal and seal with inner land groove (c_g= 15c), 10000 rpm, 70 bar [7]. Predictions for smooth seal and seal with inner land groove using (c_η = 7c)

Figure 17 depicts the seal leakage versus static journal eccentricity for operation at 10,000 rpm and 70 bar feed pressure. There is good correlation between experiments and predictions with a variation of less than ~15 % for both seals. The good correlation indicates that the selected boundary conditions represent well the physical boundaries of

the through flow. Note that the experiments and predictions show that the smooth seal leaks more than the grooved seal because its effective viscosity (land clearance) is slightly lower (larger) due to larger power losses inducing a temperature rise.

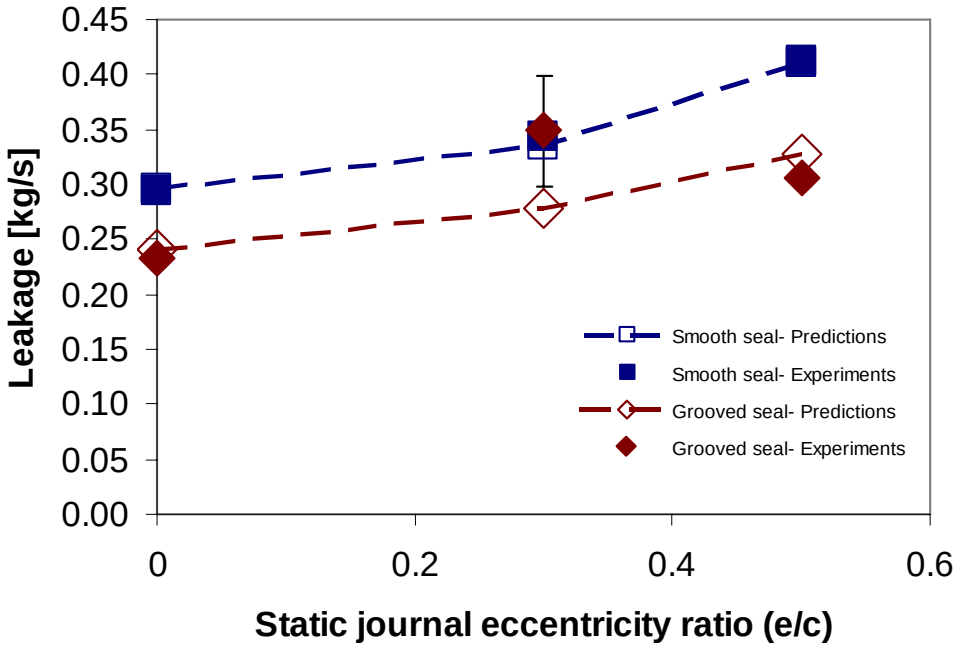

Figure 17 Seal leakage versus eccentricity. Experiments for smooth seal and seal with inner land groove (c_g= 15c), 10000 rpm, 70 bar [7]. Predictions for smooth seal and seal with inner land groove using (c_η = 7c)

V Conclusions and Recommendations

This report presents a bulk-flow formulation to obtain fluid film forces developed in grooved oil seals and details the implementation of a finite element method to obtain the force coefficient for journal off-centered operation. The current analysis extends an original bulk-flow model [8] developed for small amplitude journal motions about a centered position. The present analysis also predicts added mass coefficients, largely ignored in previous analyses of laminar-flow oil seals.

The force coefficients, leakage and reaction forces of a smooth and grooved oil seal are predicted and compared to experimental results reported in Ref. [7]. The test grooved oil seal includes a rectangular central groove located at the seal mid-land plane with a

depth of 15 times the seal clearance (c=85.9 μm). The predicted parameters are compared to experimental results for four journal eccentricities (e/c=0, 0.3, 0.5, 0.7) at 10,000 rpm and with a 70 bar oil feed pressure.

Predicted and experimental force coefficients present good correlation for the direct force coefficients for the lower journal eccentricities (e/c=0,0.3) and moderate to good correlation for e/c=0.5. The cross-coupled stiffness coefficients are also accurately predicted for the lower journal eccentricities. In particular, the current model accurately predicts the reduction of the direct stiffness, direct damping, and cross-coupled stiffness coefficients when adding a circumferential groove to the seal land. The added mass coefficients for both seals are also predicted accurately (within 20 %). Furthermore, the analysis and experimental results indicate that a grooved seal shows larger direct added mass coefficient than a smooth seal.

For journal eccentricity ratios (ε) up to 70% there are discrepancies between the experimental results and (current) predictions for some of the force coefficients. These discrepancies are attributed to (unknown) changes in seal clearance and oil viscosity induced by thermal effects when operating at large eccentricities. Nevertheless, the test data reported in Ref. [7] does not offer enough details on operating conditions and the variation of the lubricant properties and seal clearance. Therefore, the predictions are compared with experimental results only for the low to mid-range eccentricities (i.e. ε= 0, 0.3, 0.5).

The current analysis represents a significant improvement over the current predictive tools available to analyze grooved oil seals. More importantly, the improved predictions of the grooved oil seal force coefficients can lead to a more accurate estimation of critical speeds and stability thresholds in centrifugal compressors.

VI References

[1] Childs, D. W. Rodriguez, L. E., Cullotta, V., Al-Ghasem, A., and Graviss, M., 2006, "Rotordynamic-Coefficients and Static (Equilibrium Loci and Leakage) Characteristics for Short, Laminar-Flow Annular Seals," J. Tribol., **128**(2), pp. 378-387

[2] Kirk, R., 1986, "Oil Seal Dynamic Considerations for Analysis of Centrifugal Compressors," *Proc. 15th Turbomachinery Symposium*, Houston, TX, pp. 25-34.

[3] Semanate, J., and San Andrés, L., 1993, "Analysis of Multi-Land High Pressure Oil Seals," STLE Tribol. Trans., **36**(4), pp 661–669

[4] Baheti, S., and Kirk, R., 1995, "Finite Element Thermo-Hydrodynamic Solution of Floating Ring Seals for High Pressure Compressors Using the Finite-Element Method," STLE Tribol. Trans., **38**, pp. 86-97.

[5] Allaire, P. E., and Kocur, J. A. Jr., 1985, "Oil Seal Effects and Subsynchronous Vibrations in High-Speed Compressors," NASA Conf. Publ., pp. 205-223

[6] Childs, D. W., Graviss, M., and Rodriguez, L. E., 2007, "The Influence of Groove Size on the Static and Rotordynamic Characteristics of Short, Laminar-Flow Annular Seals," ASME J. Tribol, **129**(2), 398-406.

[7] Graviss, M., 2005, "The Influence of a Central Groove on Static and Dynamic Characteristics of an Annular Liquid Seal with Laminar Flow," M.S. Thesis, Texas A&M Univ., College Station, TX.

[8] San Andrés, L., and Delgado, A., 2007, "Parameter Identification of an End Sealed SFD Part II: Improved Predictions of Added Mass Coefficients for Grooved SFDs and Oil Seals," TRC report, TRC-SFD-2-06, Jun.

[9] Childs, D., 1993, *Turbomachinery Rotordynamics,* John Wiley & Sons, Inc., NY, Chap. 3.

[10] Kaneko, S., Hori, Y., and Tanaka, M., 1984, "Static and Dynamic Characteristics of Annular Plain Seals," *Proc. Third IMechE Int. Conf. Vibrations in Rotating Machinery*, York, England, Sep., pp. 205-214.

[11] Zirkelback, N., and San Andrés, L., 1996, "Bulk-Flow Model for the Transition to Turbulence Regime in Annular Seals," STLE Tribol. Trans., **39**(4), pp. 835–842.

[12] Reinhardt, F., and Lund, J. W., 1975, "The Influence of Fluid Inertia on the Dynamic Properties of Journal Bearings," ASME J. Lubr. Technol., **97**(1), pp. 154-167.

[13] San Andrés, L., "Modern Hydrodynamic Lubrication Theory," Tribology Group, Texas A&M University, http://phn.tamu.edu/me626. [accessed April 2008]

[14] San Andrés, L., 2007, " Modern Lubrication Notes # 7-Analysis of Finite Length Bearings: Reaction Forces and Dynamic Force Coefficients Including Temporal Fluid Inertia Effects," Internal Communication, Tribology Group

[15] Reddy J. N., Gartling, D. K., 2001, *The Finite Element Method in Heat transfer and Fluid Dynamics*, CRC Press, Florida, Chap. 2.